


Bioinspired Design of Vascular Artificial Muscle

Qiguang He, Zhijian Wang, Zhaoqiang Song, and Shengqiang Cai*

Recently, liquid crystal elastomers (LCEs) have drawn much attention for its wide applications as artificial muscle in soft robotics, wearable devices, and biomedical engineering. One commonly adopted way to trigger deformation of LCEs is using embedded heating elements such as resistance heating wires and photothermal particles. To enable the material to recover to its unactuated state, passive and external cooling is often employed to lower the temperature, which is typically slow and environmentally sensitive. The slow and uncontrollable recovery speed of thermally driven artificial muscle often limits its applications when even moderate cyclic actuation rate is required. In this article, inspired by biology, a vascular LCE-based artificial muscle (VLAM) is designed and fabricated with internal fluidic channel in which the hot or cool water is injected to heat up or cool down the material to achieve fast actuation as well as recovery. It is demonstrated that the actuation stress, strain, and cyclic response rate of the VLAM are comparable to mammalian skeletal muscle. Because of the internal heating and cooling mechanism, VLAM shows a very robust actuating performance within a wide range of environmental temperatures. The VLAM designed in this article may also provide a convenient way to harvest waste heat to conduct mechanical work.

Soft and stretchable actuators, which are also often called artificial muscle, have been widely employed in the applications ranging from soft robotics,^[1–3] biomimetic systems^[4–6] to wearable devices.^[7,8] Recently, various materials and structures have been explored as artificial muscle with different characteristics.^[9–14] For instance, dielectric elastomer films can generate fast and large deformation when subjected to electrical voltage;^[10–12] shape memory polymer can change shapes upon the change of temperature;^[13] environmentally sensitive hydrogels can significantly swell or shrink when exposed to different external stimuli such as the variation of temperature and pH value in a solution.^[9] Large actuating stress and strain have been recently demonstrated in thermally powered twisted fish-line artificial muscle.^[15,16] Various balloon-like structures have also been intensively explored as pneumatic and hydraulic artificial muscle in soft robots.^[17–19]

Q. He, Dr. Z. Wang, Z. Song, Prof. S. Cai
Department of Mechanical and Aerospace Engineering
University of California, San Diego
La Jolla, CA 92093, USA
E-mail: shqcai@ucsd.edu
Prof. S. Cai
Materials Science and Engineering Program
University of California, San Diego
La Jolla, CA 92093, USA

 The ORCID identification number(s) for the author(s) of this article can be found under <https://doi.org/10.1002/admt.201800244>.

DOI: 10.1002/admt.201800244

Though tremendous success has been achieved in the applications of those materials as artificial muscle, certain limitations have also been well recognized. For example, ultrahigh voltage is often required to actuate a thin dielectric elastomer film.^[11] Special designs are often required for soft pneumatic/hydraulic actuators to generate high-force output.^[20,21] Significant reduction of the size of twisted fish-line artificial muscle can be technically challenging.

Liquid crystal elastomer (LCE), as a newly emerging soft actuating material, has recently received much attention.^[22–32] Based on the molecular structure, LCE can be simply viewed as an integration of mesogenic molecules into a polymer network (Figure S1, Supporting Information). When the temperature of the LCE is increased above a critical temperature (also called isotropic transition temperature), the mesogens can transit from liquid crystal phase to isotropic phase,

which may lead to large and reversible deformation of the elastomer. It has been shown that both actuating strain and stress generated by an LCE can be comparable to real mammalian skeletal muscle.^[33] In addition, using different fabrication techniques such as 3D printing^[34] and photolithography,^[28] active LCE structures of various sizes have been successfully fabricated.

In practical uses of LCE as artificial muscle in the structures with complex forms, it is often essential to integrate heating element into the material.^[35,36] For instance, Thomsen et al. fabricated a multilayer LCE structure with embedded flexible heating element, where low-voltage-induced large deformation has been achieved. In most previous studies, resistance heating wires have been embedded into LCE, and Joule heating generated by the resistance heating wires can induce the actuation of the material. As a matter of fact, using embedded resistance heating wires to generate thermal actuation has been explored in many different thermally actuating materials including shape memory polymers,^[37] temperature-sensitive hydrogels,^[38] and fish-line artificial muscle.^[39] However, such experimental setup may have several drawbacks: First, the heating wires are typically metallic, which may constrain the stretchability and also increase the overall stiffness of the actuating material; second, for those thermally actuating materials, they are often required to recover to their initial states after being cooled down for a subsequent actuation cycle. Compared to heating up, cooling down is generally more challenging to control. So far, few efforts have been made to achieve active and fast cooling of those materials. Consequently, in most of the previous

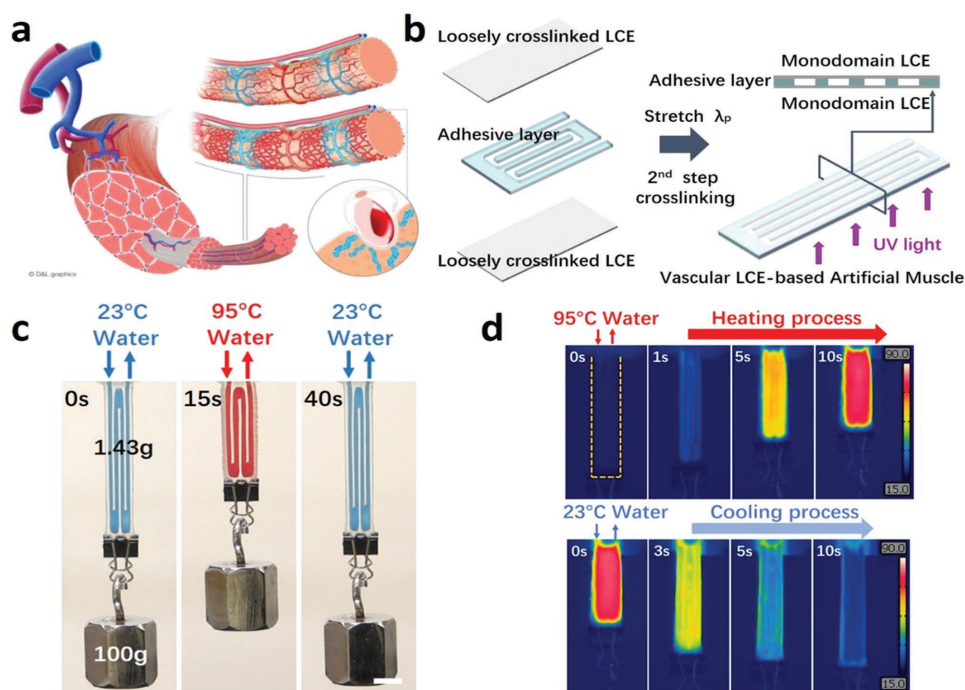


Figure 1. Design, fabrication, and performance of VLAM. a) Vascular structure of a real muscle bundle.^[42] b) Fabrication procedure of VLAM: one adhesive layer (with laser-cut water channel) is first sandwiched between two layers of loosely cross-linked LCE films; the entire structure is then stretched by λ_p and exposed under UV irradiation to form additional crosslinks in the LCE films. c) Reversible actuation of VLAM: VLAM of 1.4 g can lift up a weight of 100 g by 40% contracting strain with the injection of 95 °C circulated water (dyed red) and lower down the load with the injection of room-temperature circulated water (23 °C). Scale bar: 1 cm. d) Thermal imaging of VLAM during the contraction and recovery process.

experiments, passive and external air cooling is adopted, which is typically very slow and can greatly depend on the environmental temperature as well as the ventilating conditions.

Nevertheless, for real muscle in biology, to maintain their normal physiological activities, both the supply of oxygen and nutrients and removal of waste such as carbon dioxide^[40,41] should be highly efficient. In addition, most mass transport processes in biological system are through slow diffusion. To enable fast mass transport, the strategy adopted in nature (for both animals and plants) is to develop vascular structure (see **Figure 1a** as an example^[42]). Inspired by the prevalence of the vascular structure in biology, in the article, we design a vascular LCE-based artificial muscle (VLAM). We inject hot and cool water into its internal fluidic channel to realize both fast thermal actuation and recovery. Because of the internal heating and cooling, the VLAM shows very robust actuation performance within a wide range of environmental temperature.

We fabricate the VLAM following the steps as sketched in **Figure 1b**. The VLAM is composed of three layers. Both the top and bottom layers are monodomain LCE thin films (liquid crystal mesogens are well aligned in the film in stress-free state), while the middle layer is an adhesive thin film (VHB tape, 3M) with fluidic channel which is made by high-precision laser cutting (Universal Laser Systems).

To fabricate the VLAM, we first synthesize two loosely cross-linked polydomain LCE films, which are then bonded by an adhesive layer (VHB tape from 3M company) with laser-cut fluidic channels. The detailed synthetic procedures of the LCE film

are described in the Experimental Section. We then prestretch the entire structure by λ_p times of its original length to induce the polydomain-to-monodomain transition of the LCE and place it under UV irradiation to induce second cross-linking reaction in the LCE to fix it in monodomain state (**Figure 1b**). In the following experiments, the prestretch ratio λ_p is set to be three unless otherwise specified.

It is known that monodomain LCE can exhibit reversible thermal actuation with or without externally applied stress. When the temperature is above the isotropic transition temperature, well-aligned mesogens in the LCE can transit to isotropic state, resulting in macroscopic contraction of the elastomer along the aligning direction of mesogens. In the experiment, to increase the temperature of the VLAM, we inject hot water into its internal fluidic channel as shown in **Figure 1c** and **Movie S1** in the Supporting Information. The temperature of the hot water (dyed red) in the test is 95 °C with the flow rate of 1.50 mL s⁻¹. The VLAM with a weight of 1.43 g can contract by 40% of its initial length and lift a weight of 100 g within 10 s as shown in **Figure 1c** and **Movie S1** in the Supporting Information.

To enable the VLAM to recover to its initial length, we inject water of room temperature (dyed blue) into the internal fluidic channel. In contrast to external and passive cooling method used in most previous studies, we here adopt internal and active cooling method to lower down the temperature of the VLAM. As shown in **Figure 1c** and **Movie S1** in the Supporting Information, the artificial muscle recovers to its initial length also around 10 s, which is much faster than the external and

passive air cooling. Compared to other method to induce active deformation of LCEs such as light and resistance heating wires, using circulating water provides another potential advantage: the artificial muscle can keep its high transparency during the entire actuating process as shown in Figure S2 in the Supporting Information.

During the process of injecting water into the VLAM, we use thermal imaging technique (FLIR E75-42 Advanced Thermal Imaging Camera) to further examine the temperature of the surface of VLAM as shown in Figure 1d and Movie S2 in the Supporting Information. When we inject hot water of 95 °C into the fluidic channel of the artificial muscle, the surface temperature of the structure increases from 20 to 85 °C within 10 s and then maintain as a constant, indicating the temperature field in the material reaches a steady state. Likewise, the temperature decreases from 85 to 20 °C also

within 10 s, when water of room temperature is injected into the VLAM.

We next quantitatively characterize the dynamics of actuation of VLAM. In the experiment, we first measure the actuation strain of a free-standing VLAM with the injection of hot water into its internal fluidic channel. The results are shown in Figure 2a. The actuation strain increases rapidly and reaches a plateau value within 8 s after the injection of hot water at 95 °C with the flow rate of 1.50 mL s⁻¹. When the actuation strain reaches the plateau, the VLAM reaches a steady state. Depending on the temperature of the injected water, the plateau value varies. After the actuation strain stays at the maximal value for tens of seconds, we inject water of room temperature (23 °C) into VLAM with the flow rate of 1.50 mL s⁻¹. As shown in Figure 2b, around 15 s after the injection of cool water, the VLAM recovers to its initial state, which is much faster than

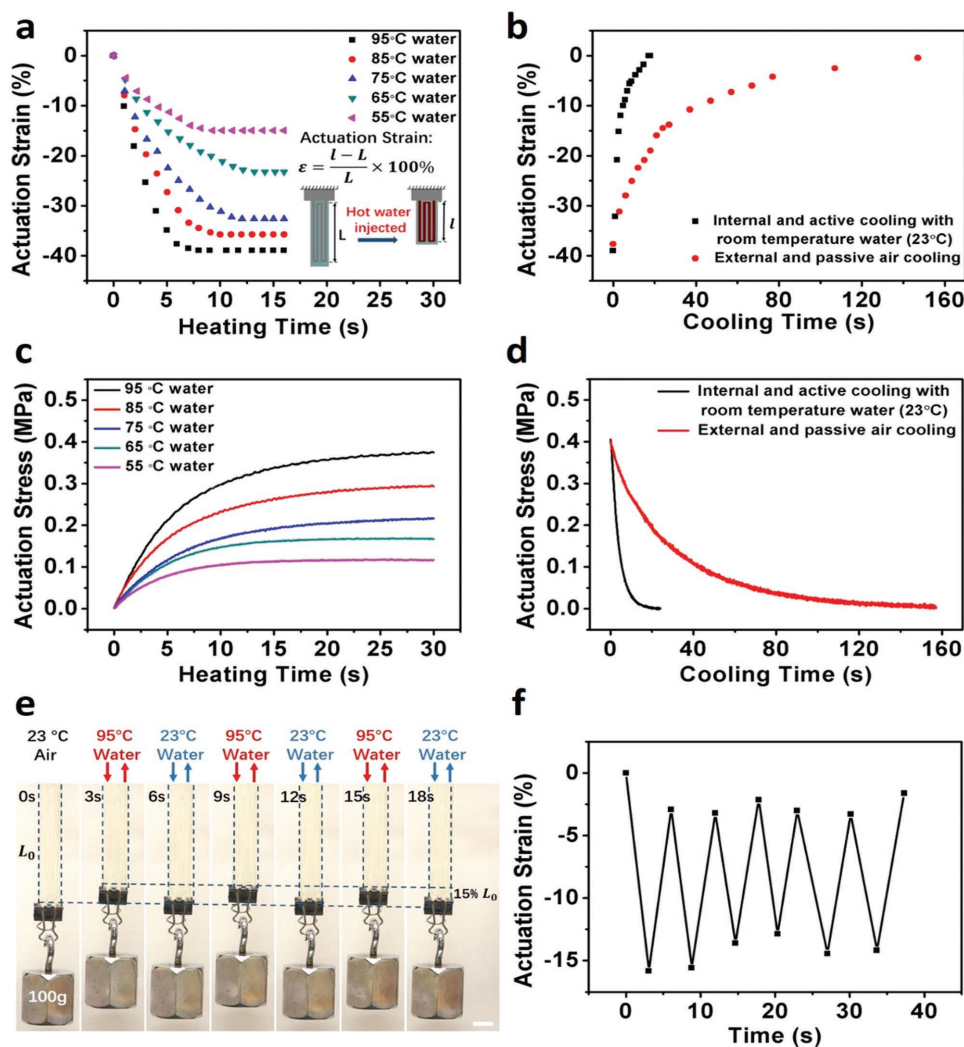


Figure 2. Fast actuation and recovery of VLAM. a) Actuation strain of a free-standing VLAM as a function of time with the injection of water at several different temperatures. b) Recovery of an actuated free-standing VLAM as a function of time through internal and active cooling with room-temperature water and through external and passive air cooling. c) Actuation stress of VLAM with fixed length as a function of time with the injection of water at several different temperatures. d) Stress relaxation of an actuated VLAM with fixed length as a function of time through internal and active cooling with room-temperature water injection and through external and passive air cooling. e, f) Fast cyclic actuation and recovery of a VLAM attached to a weight of 100 g, with the alternative injection of room-temperature water and hot water. Scale bar in panel (e) is 1 cm.

the passive and external air cooling as also shown in Figure 2b for comparison. As discussed previously, slow recovery process often limits the applications of most thermally driven artificial muscle.

By fixing its original length, we can also measure the actuating stress generated by the VLAM when hot or cool water is injected into it. Similar to the change of actuation strain, as shown in Figure 2c, the actuation stress increases rapidly from zero to a maximal value within 30 s. The maximal actuating stress also depends on the temperature of the hot water. The actuation stress quickly relaxes to zero (within 15 s) when we inject cool water into the structure as shown in Figure 2d.

In addition to the temperature of the water, we also study the effect of flow rate of the water on the actuating performance of VLAM. The results are shown in Figure S3 in the Supporting Information. In the experiment, the temperature of the hot water is fixed at 95 °C and the cool water is fixed at room temperature, and we use three different flow rates: 1.5, 1.0, and 0.5 mL s⁻¹. With the increase of the flow rate, both the thermal actuation and recovery of VLAM are faster. The flow rate of water has negligible influence on the magnitudes of actuating stress and actuating strain of VLAM in steady state.

By alternatively injecting room-temperature water and hot water into VLAM, we further demonstrate that the frequency of cyclic actuation (with an actuation strain of 15%) of VLAM can be easily achieved at around 0.2 Hz as shown in Figure 2e,f and Movie S3 in the Supporting Information, without detailed structural optimization and using fluids at extreme temperatures. According to our knowledge, such cyclic response rate is significantly faster than most thermally actuating materials

with similar level of actuation strain and size, reported in the previous studies.^[3,38,43] In addition, the cyclic response rate of VLAM is also close to that of mammalian skeletal muscle.^[40] It is also noted that we did not detect any water leakage or film delamination after 30 cycles of actuation.

The actuation performance of VLAM strongly depends on the prestretch ratio λ_p during the second cross-linking step of the LCE (Figure 1b). To study such dependence, we prestretch loosely cross-linked LCE films by λ_p of three different values: 2.0, 2.5, 3.0, and then crosslink the film under the illumination of UV light during the fabrication procedure as shown in Figure 1b. We measure the actuation strain and stress of VLAM in the steady state with the injection of water at different temperatures (from 40 to 95 °C). We plot the experimental measurements of actuation strain and stress in Figure 3a,b. With the increase of the prestretch λ_p or the temperature of the injected water, the magnitude of both actuation strain and actuation stress increase. In particular, as the temperature of water is increased from 40 to 95 °C, the magnitude of actuation strain increases from 7% to 40%, and the magnitude of actuation stress increases from 0.1 to 0.4 MPa for VLAM with the prestretch $\lambda_p = 3$. Both actuation stress and strain are comparable to those of mammalian skeletal muscle (with actuation strain ranging from 20% to 40% and actuation stress ranging from 0.10 to 0.35 MPa^[40]). It is also worth to mention that the actuation strain of VLAM is almost identical to a single monodomain LCE sheet with the same prestretch λ_p (Figure S4, Supporting Information), implying that the embedded fluidic channel does not place any restriction on the actuation capacity of active LCE films.

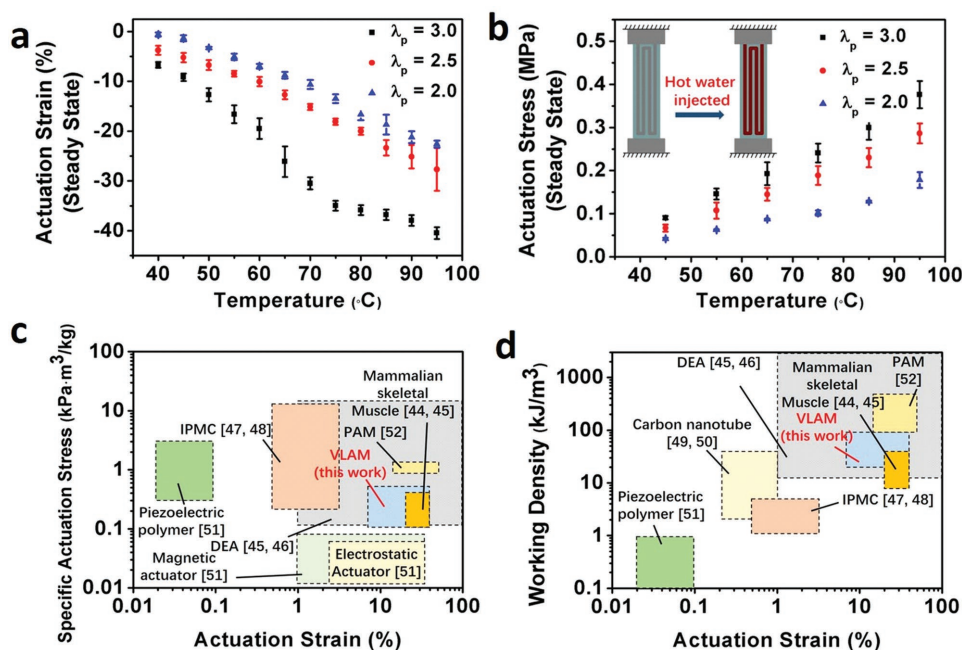


Figure 3. Actuation performances of VLAM at steady state. a) Actuation strain of free-standing VLAM as a function of temperature, for three different prestretch ratios of the VLAM: $\lambda_p = 2.0, 2.5,$ and 3.0 , during its preparation. b) Actuation stress of VLAM with fixed length as a function of temperature for three different prestretch ratios of the VLAM: $\lambda_p = 2.0, 2.5,$ and 3.0 , during its preparation. c) Specific actuation stress versus actuation strain of several widely used actuating materials and mammalian skeletal muscle. d) Working density versus actuation strain of several widely used actuating materials and mammalian skeletal muscle. VLAM, vascular LCE-based artificial muscle. IPMC, ionic polymer metal composite. DEA, dielectric elastomer actuator. PAM, pneumatic artificial muscle.

In Figure 3c, we plot the specific actuation stress (actuation stress divided by density) versus the magnitude of actuation strain of VLAM based on the measurements in Figure 3a,b, together with other widely used actuating materials and mammalian skeletal muscle.^[44–52] In Figure 3d, we plot the working density of the VLAM based on the experimental measures shown in Figure 1c and Figure S5 in the Supporting Information, in which we hang weight of 100 and 500 g at the bottom of a VLAM, respectively, and measure the corresponding contracting distance of the artificial muscle with the injection of hot water of 95 °C. We find that in terms of the performance metrics in Figure 3c,d, VLAM is comparable to mammalian skeletal muscle. VLAM also has similar actuation performance as currently leading artificial muscle materials: dielectric elastomer and pneumatic artificial muscle. Considering many other advantageous features, VLAM can be regarded as excellent supplement to all the currently available artificial muscle materials for various applications.

Performance of most thermally driven artificial muscle can strongly depend on the environmental temperature. Thanks to the internal cooling and heating mechanism, another important advantage of VLAM developed in this article is its broad range of working temperature. In the experiment, we submerge a VLAM into a large water tank with temperature ranging from 5 to 80 °C as shown in Figure 4a,b. It is noted that thermal contraction in an LCE film becomes noticeable

when its temperature is above 40 °C and reaches maximum when the temperature is 80 °C. Consequently, in our experiment, when the VLAM is put into the water tank of temperature above 40 °C, it shortens immediately. We plot the ratio of the length of the VLAM in the air (L_{air}) and in the water tank (L_w) of different temperatures in Figure 4c. It clearly shows that in the water tank of 80 °C, the artificial muscle can contract as much as 40%. We then alternatively inject hot water (95 °C) and cool water (5 °C) into the VLAM to investigate its actuating behavior. We plot the length of the artificial muscle L_c (normalized by L_{air}) in the steady state with the injection of cool water in Figure 4d. We also plot the actuation strain of the VLAM in Figure 4d, which is defined as $(L_c - L_h)/L_c$, where L_h is the length of VLAM in the steady state with the injection of hot water. As we can see from Figure 4d, the magnitude of the actuation strain is roughly a constant for the entire range of experimental temperature (5–80 °C).

As a final demonstration, we use VLAM to drive different modes of motion of a skeleton model. The attachments of artificial femoris, biceps, triceps, and masseter muscles onto the skeleton are shown in Figure 5 and Movie S4 in the Supporting Information. With hot water (95 °C) injected to the artificial masseter muscles, they contract, move the jaw up, and close the mouth. The mouth can quickly open with cold water being injected into the artificial masseter muscle. The bending movement of elbow can be controlled by two separate muscles: biceps and triceps.

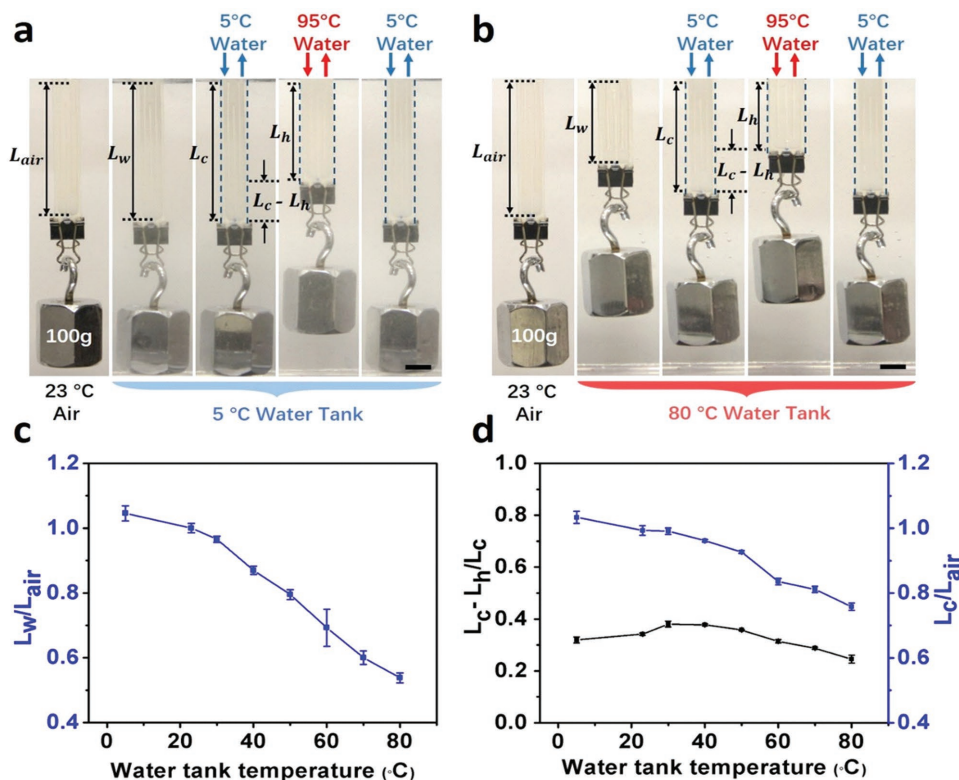


Figure 4. Actuation of VLAM in a wide range of environmental temperature. a) Reversible actuation of a VLAM in cold water (5 °C). b) Reversible actuation of a VLAM in hot water (80 °C). c) Length of a VLAM (normalized by its length in the air) in a water tank at different temperatures. d) Length of a VLAM in a water tank with the injection of cold water (5 °C), and the actuation strain of the VLAM with injection of hot water (95 °C). The magnitude of actuation strain only weakly depends on the environmental temperature indicating the high robustness of the system. Scale bar in panels (a) and (b) are 1 cm.

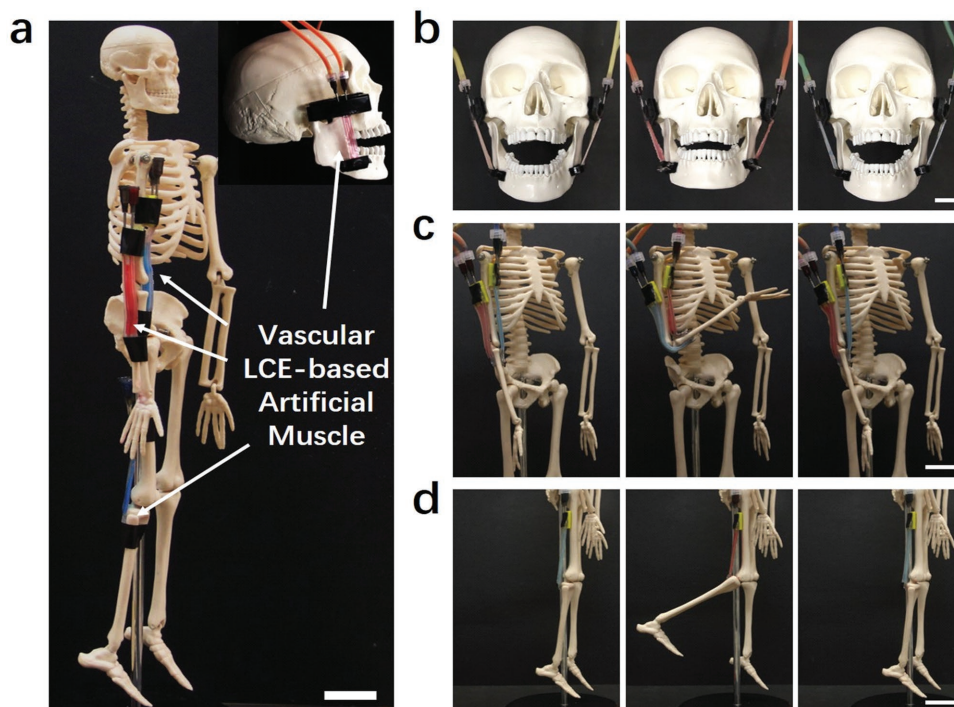


Figure 5. a) Demonstration of the implementation of VLAM as biceps femoris artificial muscle, biceps artificial muscle, triceps artificial muscle, and masseter artificial muscle on a human skeleton. b) Jaw movement by contraction of artificial masseter muscle. c) Lift of an arm by the contraction of artificial biceps muscle and relaxation of artificial triceps muscle. d) Lift of a shank by the contraction of artificial biceps femoris muscle. The scale bars in all the figures are 2 cm.

We simultaneously inject hot and cool water into artificial biceps and triceps muscles, respectively. The biceps contract and triceps relax, which moves the arm to bend at elbow. Alternately injecting hot and cool water can generate cyclical movement of the arm. The artificial muscle can also be used as biceps femoris to control the movement of the shank of the skeleton.

In conclusion, in the article we demonstrate a bioinspired design of a vascular LCE-based artificial muscle, which exhibits large actuation strain and stress in a fast-cyclic response rate. In many aspects, the actuating performance of the artificial muscle is comparable to real mammalian skeleton muscles. Thanks to the internal heating and cooling by circulated water, the newly developed artificial muscle can work in a broad range of environmental temperatures while maintaining robust performance. We further demonstrate the application of the vascular artificial muscle in driving various movements of a skeleton. Last, we would like to point out that the fluid-driven vascular artificial muscle developed in this article may provide an effective way to make use of waste heat generated in different processes. Although in this article, we only demonstrate the advantages of the vascular structure in the LCE-based artificial muscle, similar ideas should be applicable to most thermally actuating materials of various kinds.

Experimental Section

Materials and Methods: (1,4-bis-[4-(3-acryloyloxypropyloxy) benzoyloxy]-2-methylbenzene) (RM257) (Wilshire Company, 95%), 2,2'-(ethylenedioxy) diethanethiol (EDDET, Sigma-Aldrich, 95%), pentaerythritol tetrakis (3-mercaptopropionate) (PETMP, Sigma-Aldrich, 95%),

dipropylamine (DPA, Sigma-Aldrich, 98%), (2-hydroxyethoxy)-2-methylpropiophenone (HHMP, Sigma-Aldrich, 95%), VHB (3M, 4910), Epoxy (Loctite Epoxy 1 min), and toluene were used as received without further purification. The flow rate of water was precisely controlled by syringe pump (Cole-Parmer, USA). Instron Universal Testing System (5965 Dual Column Testing Systems, Instron) with 5 kN loading cell was used to conduct mechanical measurements. The photos and videos in this work were taken by digital camera (Canon 60D).

Preparation of Loosely Cross-Linked LCE: The LCE films were prepared following modified procedures of previous work.^[53] RM257 (10.956 g, 18.6 mmol) was dissolved in toluene and the mixture is placed in 85 °C for 20 min. Then, the photoinitiator HHMP (0.077 g, 0.3 mmol) was added into the mixture and heated to be dissolved. EDDET (3.076 g, 16.9 mmol), the spacer in LCE and the tetra-arm thiol crosslinker, and PETMP (0.244 g, 0.5 mmol) were added into the mixture. After that, the catalyst DPA (0.038 g, 0.4 mmol) was added into mixture. The mixture was stirred and degassed in the vacuum chamber to remove the bubbles. Then, the mixture was poured into a rectangular mold with 1 mm thickness. After 24 h, the LCE films were put into 85 °C oven for 12 h to evaporate solvent. Then, the loosely cross-linked LCE was obtained.

Fabrication of VLAMs: VHB (3M, 4910) stretchable tape was used as middle layer for its strong adhesion with LCE film. The fluidic channel in the VHB was created using laser cutting system (Universal Laser Systems). The stretchable tape (with fluidic channels) was placed between two layers of loosely cross-linked LCE films forming sandwich-like structure; then, the whole structure is stretched by λ_p (2.0, 2.5, and 3.0) to different lengths. After placing under UV irradiation for 2 h, the VLAM was made. The top of artificial muscle was fixed on glass substrate. A total of 16 gauge (Bstean) industrial needles were inserted into fluid channel and epoxy (Loctite) was used to seal the connecting joint parts.

Supporting Information

Supporting Information is available from the Wiley Online Library or from the author.

Acknowledgements

The authors acknowledge support from the National Science Foundation through Grant No. CMMI-1554212 and ONR through Grant No. N00014-17-1-2056.

Conflict of Interest

The authors declare no conflict of interest.

Keywords

artificial muscle, liquid crystal elastomer, vascular structure

Received: July 3, 2018

Revised: August 29, 2018

Published online:

- [1] D. Rus, M. T. Tolley, *Nature* **2015**, 521, 467.
- [2] M. T. Tolley, R. F. Shepherd, B. Mosadegh, K. C. Galloway, M. Wehner, M. Karpelson, R. J. Wood, G. M. Whitesides, *Soft Rob.* **2014**, 1, 213.
- [3] A. Miriyev, K. Stack, H. Lipson, *Nat. Commun.* **2017**, 8, 596.
- [4] A. D. Marchese, C. D. Onal, D. Rus, *Soft Rob.* **2014**, 1, 75.
- [5] C. Laschi, M. Cianchetti, B. Mazzolai, L. Margheri, M. Follador, P. Dario, *Adv. Rob.* **2012**, 26, 709.
- [6] H. Zeng, O. M. Wani, P. Wasylczyk, A. Priimagi, *Macromol. Rapid Commun.* **2018**, 39, 1700224.
- [7] M. Wehner, M. T. Tolley, Y. Mengüç, Y.-L. Park, A. Mozeika, Y. Ding, C. Onal, R. F. Shepherd, G. M. Whitesides, R. J. Wood, *Soft Rob.* **2014**, 1, 263.
- [8] E. C. Goldfield, Y.-L. Park, B.-R. Chen, W.-H. Hsu, D. Young, M. Wehner, D. G. Kelty-Stephen, L. Stirling, M. Weinberg, D. Newman, *Ecol. Psychol.* **2012**, 24, 300.
- [9] Y. Liu, K. Zhang, J. Ma, G. J. Vancso, *ACS Appl. Mater. Interfaces* **2016**, 9, 901.
- [10] C. Keplinger, J.-Y. Sun, C. C. Foo, P. Rothemund, G. M. Whitesides, Z. Suo, *Science* **2013**, 341, 984.
- [11] E. Acome, S. Mitchell, T. Morrissey, M. Emmett, C. Benjamin, M. King, M. Radakovitz, C. Keplinger, *Science* **2018**, 359, 61.
- [12] N. Kellaris, V. G. Venkata, G. M. Smith, S. K. Mitchell, C. Keplinger, *Sci. Rob.* **2018**, 3, eaar3276.
- [13] X. Kuang, K. Chen, C. K. Dunn, J. Wu, V. C. Li, H. J. Qi, *ACS Appl. Mater. Interfaces* **2018**, 10, 7381.
- [14] D. Yang, M. S. Verma, J. H. So, B. Mosadegh, C. Keplinger, B. Lee, F. Khashai, E. Lossner, Z. Suo, G. M. Whitesides, *Adv. Mater. Technol.* **2016**, 1, 1600055.
- [15] C. S. Haines, M. D. Lima, N. Li, G. M. Spinks, J. Foroughi, J. D. Madden, S. H. Kim, S. Fang, M. J. de Andrade, F. Göktepe, *Science* **2014**, 343, 868.
- [16] S. M. Mirvakili, A. R. Ravandi, I. W. Hunter, C. S. Haines, N. Li, J. Foroughi, S. Naficy, G. M. Spinks, R. H. Baughman, J. D. Madden, presented at *Electroactive Polymer Actuators and Devices (EAPAD)*, San Diego, CA, March **2014**.
- [17] S. Terryn, J. Brancart, D. Lefeber, G. Van Assche, B. Vanderborght, *Sci. Rob.* **2017**, 2, eaan4268.
- [18] H. Yuk, S. Lin, C. Ma, M. Takaffoli, N. X. Fang, X. Zhao, *Nat. Commun.* **2017**, 8, 14230.
- [19] S. Li, D. M. Vogt, D. Rus, R. J. Wood, *Proc. Natl. Acad. Sci. USA* **2017**, 114, 13132.
- [20] C.-P. Chou, B. Hannaford, *IEEE Trans. Rob. Autom.* **1996**, 12, 90.
- [21] H. K. Yap, H. Y. Ng, C.-H. Yeow, *Soft Rob.* **2016**, 3, 144.
- [22] M. A. Robertson, H. Sadeghi, J. M. Florez, J. Paik, *Soft Rob.* **2017**, 4, 23.
- [23] Z. Wang, H. Tian, Q. He, S. Cai, *ACS Appl. Mater. Interfaces* **2017**, 9, 33119.
- [24] Z. Pei, Y. Yang, Q. Chen, E. M. Terentjev, Y. Wei, Y. Ji, *Nat. Mater.* **2014**, 13, 36.
- [25] S. Palagi, A. G. Mark, S. Y. Reigh, K. Melde, T. Qiu, H. Zeng, C. Parmeggiani, D. Martella, A. Sanchez-Castillo, N. Kapernaum, *Nat. Mater.* **2016**, 15, 647.
- [26] H. Zeng, O. M. Wani, P. Wasylczyk, R. Kaczmarek, A. Priimagi, *Adv. Mater.* **2017**, 29, 1701814.
- [27] Y. Xia, G. Cedillo-Servin, R. D. Kamien, S. Yang, *Adv. Mater.* **2016**, 28, 9637.
- [28] A. H. Gelebart, D. J. Mulder, M. Varga, A. Konya, G. Vantomme, E. Meijer, R. L. Selinger, D. J. Broer, *Nature* **2017**, 546, 632.
- [29] Z. Wang, W. Fan, Q. He, Y. Wang, X. Liang, S. Cai, *Extreme Mech. Lett.* **2017**, 11, 42.
- [30] Q. Li, *Liquid Crystals Beyond Displays: Chemistry, Physics, and Applications*, John Wiley & Sons, Hoboken, NJ **2012**.
- [31] Q. Li, *Intelligent Stimuli-Responsive Materials: From Well-Defined Nanostructures to Applications*, John Wiley & Sons, Hoboken, NJ **2013**.
- [32] H. K. Bisoyi, Q. Li, *Chem. Rev.* **2016**, 116, 15089.
- [33] H. Tian, Z. Wang, Y. Chen, J. Shao, T. Gao, S. Cai, *ACS Appl. Mater. Interfaces* **2018**, 10, 8307.
- [34] C. P. Ambulo, J. J. Burroughs, J. M. Boothby, H. Kim, M. R. Shankar, T. H. Ware, *ACS Appl. Mater. Interfaces* **2017**, 9, 37332.
- [35] D. L. Thomsen, G. Bush, P. Keller, R. G. Bryant, *SPIE's 9th Ann. Int. Symp. Smart Struct. Mater.: Electroact. Polym. Actuators Device* **2002**, 4695, 435.
- [36] C. Wang, K. Sim, J. Chen, H. Kim, Z. Rao, Y. Li, W. Chen, J. Song, R. Verduzco, C. Yu, *Adv. Mater.* **2018**, 30, 1706695.
- [37] S. Felton, M. Tolley, E. Demaine, D. Rus, R. Wood, *Science* **2014**, 345, 644.
- [38] C. Yu, Z. Duan, P. Yuan, Y. Li, Y. Su, X. Zhang, Y. Pan, L. L. Dai, R. G. Nuzzo, Y. Huang, *Adv. Mater.* **2013**, 25, 1541.
- [39] S. M. Mirvakili, I. W. Hunter, *Adv. Mater.* **2017**, 29, 1604734.
- [40] J. D. Madden, N. A. Vandesteeg, P. A. Anquetil, P. G. Madden, A. Takshi, R. Z. Pytel, S. R. Lafontaine, P. A. Wieringa, I. W. Hunter, *IEEE J. Oceanic Eng.* **2004**, 29, 706.
- [41] S. Perry, *Can. J. Zool.* **1986**, 64, 565.
- [42] Y. H. Kusters, E. J. Barrett, *Am. J. Physiol.-Endocrinol. Metab.* **2015**, 310, E379.
- [43] C. Yuan, D. J. Roach, C. K. Dunn, Q. Mu, X. Kuang, C. M. Yakacki, T. Wang, K. Yu, H. J. Qi, *Soft Matter* **2017**, 13, 5558.
- [44] I. W. Hunter, S. Lafontaine, presented at *Solid-State Sensor and Actuator Workshop, 1992. 5th Technical Digest.*, Hilton Head Island, SC, June **1992**.
- [45] Y. Bar-Cohen, presented at *19th AIAA Applied Aerodynamics Conf.*, Anaheim, CA, June **2001**.
- [46] Q. Pei, M. A. Rosenthal, R. Pelrine, S. Stanford, R. D. Kornbluh, presented at *Smart Structures and Materials 2003: Electroactive Polymer Actuators and Devices (EAPAD)*, San Diego, CA, March **2003**.
- [47] T.-G. Noh, Y. Tak, J.-D. Nam, H. Choi, *Electrochim. Acta* **2002**, 47, 2341.
- [48] K. J. Kim, M. Shahinpoor, *Smart Mater. Struct.* **2003**, 12, 65.
- [49] R. H. Baughman, C. Cui, A. A. Zakhidov, Z. Iqbal, J. N. Barisci, G. M. Spinks, G. G. Wallace, A. Mazzoldi, D. De Rossi, A. G. Rinzler, *Science* **1999**, 284, 1340.
- [50] J. N. Barisci, G. G. Wallace, R. H. Baughman, *J. Electrochem. Soc.* **2000**, 147, 4580.
- [51] S. Ashley, *Sci. Am.* **2003**, 289, 52.
- [52] S. M. Mirvakili, I. W. Hunter, *Adv. Mater.* **2018**, 30, 1704407.
- [53] C. Yakacki, M. Saed, D. Nair, T. Gong, S. Reed, C. Bowman, *RSC Adv.* **2015**, 5, 18997.